A CFD Study of Bubble Dynamics and Voltage Drop in Slotted Anodes

Mostafa El Mehdi Brik[1], Ievgen Necheporenko[2] and Alexander Arkhipov[3]
1. Engineer - I R&D
2. Senior Engineer - R&D
3. Manager - Modelling
Technology Development & Transfer department, Emirates Global Aluminium, Dubai, UAE
Corresponding author: mbrik@ega.ae
https://doi.org/10.71659/icsoba2024-al043

Abstract

This paper extends our previous research (ICSOBA, 2023) by introducing the variation of bubble voltage drop during the slotted anode life span (~24 days) into the existing Computational Fluid Dynamics (CFD) model. This enhanced model investigates the gas dynamics and bubble voltage drop in an aluminium electrolysis cell. Numerical simulations for two anode slots inclinations (20 mm and 80 mm) were performed using COMSOL Multiphysics software based on the finite element method. The CFD model couples turbulent flow, phase transport, and secondary current distribution physics. The latter gives the voltage drop caused by the gas concentration and its layer thickness underneath the anode, while Navier-Stokes equations and phase transport physics give the velocity and pressure profiles as well as the gas volume fraction distribution, respectively. The standard k-ε turbulence model was used. The results reveal how different parameters vary throughout anode life span like the gas bubble voltage drop, bath mixing efficiency caused by pushing the gases towards the central channel, and heat transfer through the side wall due to the change in flow stirring, corresponding to the variation of gas amount passing to the side channel. These findings can help the optimization of slotted anode designs in industrial cells.

Keywords: Aluminium electrolysis cell, Slotted carbon anode block, CFD, Bubble-induced turbulence.

1. Introduction

During primary aluminium production, gases are generated by electrolysis underneath anodes at high temperature of about 960 °C. While these gases (typically carbon dioxide, CO_2) aid alumina dissolution and improve heat transfer within the cell, the turbulence they provoke increases bath hydrodynamics instability and their electrical insulating properties decrease the effective area for electric current flow, leading to a higher voltage requirement (voltage drop) [1-3]. This gas bubble voltage drop can be responsible for as much as 10 % of energy loss through Ohmic heating in aluminium reduction cells [4]. To minimize this energy penalty, aluminium smelters employ various strategies, one of which involves anode slots. These slots, as referenced in different experimental works and industrial trials conducted to record the impact of anode shape on the hydrodynamics and potential fluctuations [5-11], can significantly reduce the anode voltage drop and the whole pot noise compared with traditional anodes without slots. To clearly observe the released gas behaviour and evaluate its impacts on the bath hydrodynamics, while avoiding the harsh operational conditions in an electrolysis cell (high temperature, high corrosive media, and high electromagnetic field), engineers and researchers used lab-scale models using alternative liquid-gas systems instead of electrolytic CO_2 gas, based on the idea that the dynamic viscosity of some liquids at 25 °C is almost the same as that of the cryolite at 960 °C [12-16]. The researchers found that slotted anodes significantly increased the rate of bubble removal by providing a direct pathway for bubbles to rise to the surface.

The cited studies, along with others, highlight the complexity of experimentally studying bath hydrodynamics coupled with bubble voltage drop, particularly with slotted anodes, due to multiple factors. Consequently, existing experimental research often employs idealized configurations – perfectly horizontal anodes with square edges and sidewalls – which may not directly translate to real-world industrial cells. To cover these missed elements, numerical models have been developed allowing better understanding of this topic. In parallel to his experimental work using molten bath of copper sulphate ($CuSO_4$) as aqueous electrolysis solution, Sun et al. [17] have also proposed a 3D transient mathematical model that combines discrete phase model (DPM), discrete-continuum transition model (DCTM), and volume of fluid (VOF) method to track the dispersed bubble trajectory, bridge the dispersed bubble to continuous gas, and resolve the deformed bubble surface, respectively. They have shown that slots decrease the bubble diameters and reduce the residence time by shortening the bubble motion distance. They have illustrated as well that increasing electric current provokes, on one hand, an acceleration in bubble coalescence and, on the other hand, a decrease in their collision probability. In their previous work, Sun et al. [18], coupled magnetohydrodynamics and VOF model to deeply investigate the impact of slotted anodes on bubble behaviour through a 3D transient model. They demonstrated that using slotted anodes provokes an increase in the time-averaged gas bubble removal rate from 36 % to 63 % and a decrease in the bubble layer thickness by about 3.5 mm (17.4 %). Poncsák et al. [19] proposed a bubble layer simulator that models the impact of gas bubbles on voltage fluctuations in aluminium electrolysis. Their simulations revealed that well-placed slots in the anodes significantly reduce both the voltage fluctuation range and the average voltage, especially for new anodes without edge rounding. A CFD study by Zhu et al. [20] investigated the impact of slotted anodes on bath flow and alumina transport in aluminium reduction cells. Their findings indicate that slotted anodes increase the maximum flow velocity but slightly decrease the average horizontal velocity. This results in a more uniform distribution of alumina compared to unslotted anodes. Gusberti and Severo [21] investigated the impact of bubble growth, coalescence, and detachment from the bottom of anodes on the variation of bubble voltage drop. They proposed a numerical model that couples electric equations with the multiphase bath/bubble flow where the presence of gaseous phase resistance results in local current density perturbations. Their work [21] revealed a high sensitivity of bubble behavior and gas layer voltage drop to the anode geometry, inclination, as well as the slot type and number.

In our previous paper [22], a numerical model based on turbulent flow, coupled with phase transport physics was proposed with the intention of thoroughly investigating the role of slotted anodes on the evacuation of the gas phase generated at its bottom surface, the mixing in the central channel, and heat transfer in the side channel. This was obtained by evaluating the bath hydrodynamics as well as the gas phase redistribution through different channels after its generation underneath the anode, taking into account anode rounding, measured on a cut-out cell, that is produced by the concentration of the electric current at anode edges. It was shown that the more the slot is inclined towards the central channel, the higher the gas amount passing through the central channel and the less to the side channel. This decreases bath stirring in the side channel which helps the ledge stability. It was demonstrated as well that greater width of the slot helps better gas removal from the bottom of the anode, which can lead to a decrease in the gas concentration underneath.

The present paper builds upon our ICSOBA 2023 work [22] by incorporating the dynamic change in bubble voltage drop over a typical slotted anode lifespan (~72 shifts, 24 days) into our existing CFD model. This upgraded model provides a better understanding of gas behaviour and voltage drop in an aluminium electrolysis cell. The paper is structured as followed: Starting with a description of the mathematical model in the second section, the model validations with experimental data from the literature, and various configurations to be studied are then described in the first part of Section 3. Subsequently, the second part (Section 3) is devoted to discussion and analysis of different simulated cases.

2. Mathematical model

2.1 Governing Equations

The anode reaction (1) produces CO_2 bubbles that detach and rise through the bath and induce bath circulation.

$$C + 2O^{2-} \rightarrow CO_2 + 4\,e^- \quad (1)$$

According to Faraday's law, the gas flux generated underneath the anodes is proportional to the local current density and molar weight of the gas (CO_2) and inversely proportional to the number of the released electrons from the reaction (4 in reaction (1), as cited before).

To describe numerically the phenomena cited above, we have coupled our previous 3D transient CFD model [22], that resolves turbulent flow and phase transport physics, with the secondary current distribution equation to consider the impact of the imposed current distribution on the gas generated flux as well as the variation of the bubble voltage drop. From the upgraded model we can obtain the gas volume fraction distribution in the computational domain, the velocity and pressure profiles, and the variation of the gas voltage drop provoked by the generation of bubbles under anodes. This is described by the secondary current distribution equations (2), which accounts for the effect of electrode kinetics in addition to bath resistance. In the secondary current distribution interface, current density due to the electrochemical reactions is described as a function of the overpotential kinetics and implemented as a boundary condition. The classical Butler-Volmer relation, expressed with the exchange current density (i_0) is used to describe the relation between the current density and the overpotential [23, 24].

$$\vec{j}.\vec{n} = i_0\left(e^{\frac{\alpha_a F}{RT}\eta} - e^{-\frac{\alpha_c F}{RT}\eta}\right) \quad (2)$$

where:

$\vec{j}$	Current density,
i_0	Exchange current density
α_a, α_c	Anodic and cathodic transfer coefficient, respectively
F	Faraday constant $= 96486$ C/mol
T	Temperature
R	Universal gas constant
η	Overpotential

$$\eta = V - \emptyset - E_0 \quad (3)$$

where:

V	Electrode potential
$\emptyset$	Electrolyte potential
E_0	Reaction potential

The governing equations describing the turbulent flow and the phase transport physics are cited in our previous work [22].

2.2 Boundary Conditions

The boundary conditions used for the solution of the differential equations cited above are:

- Inlet mass flux of generated CO_2 at the anode surfaces in contact with the bath depending on the local current density according to Faraday's law:

$$\dot{q}_{Co_2} = \frac{M_{Co_2} \cdot J}{4 \times F} \quad (4)$$

where:
M_{Co_2} Molar weight of CO_2 gas

The rest of the boundary conditions for the CFD physics are cited in our previous work [22]:

- At the top surface of the bath, a gas flux outlet has been imposed which allows the gas to escape with inlet rate;
- Slip condition on the gas inlet and outlet;
- The remaining walls satisfy the non-slip condition.
- For slotted configurations, a slip condition is applied to the slot walls. The slot walls are assumed to be covered or partially covered with gas evacuated from the bottom surface of the anode.

Concerning the electric current physics, boundary conditions are set as follows:

- Electric current imposed at the anode surfaces in contact with the electrolyte bath;
- Electric potential V = 0 V imposed at the bottom of the ACD (referred to the upper surface of the cathode);
- The remaining boundaries are supposed to be electrically insulated.

It is worth noting that the re-oxidation reaction is excluded in the calculations. As explained in [22], these boundary conditions are used to solve the governing equations within the 3D Cartesian system. Using the commercial CFD software COMSOL Multiphysics, the continuous phase containing gas bubbles is discretized into finite elements. To optimize the computational time and memory power, a symmetry is assumed. The finite element method is used to calculate the electric potential, velocity, pressure, and volume fraction at each node. An Algebraic Multigrid Method (AMG) solver coupled with a time-dependent second-order backward differentiation formula (BDF) tackles the time stepping process. The computational domain is discretized into a mesh, composed of 2 million elements.

3. Results and Discussion

3.1 Model Validation

The model validation is made by comparing our numerical results with the experiments of Cooksey and Yang [25] for the impact of induced bubbles on the behaviour of the bath turbulent flow when using anodes with and without slots. Good agreement was found between experimental and numerical results, demonstrating the model effectiveness for both slotted and unslotted anode configuration. Different details for this part of the model validation are given in our previous work [22].

On the other hand, numerical results obtained from our model have been compared to those obtained by Gusberti et al. [21, 26] for the variation of the bubble voltage drop at the end-of-life stage for a flat and inclined anode and different applied electric currents, as shown in Table 1. Considering the same simulation parameters as used in Gusberti et al. [21], the comparison between the different results reveals a good concordance in term of gas coverage as well as bubble voltage drop. These agreements validate the model for use in subsequent analyses.

Table 1. Comparison between our results and those found by Gusberti et al. [21, 26].

Anode bottom surface = 160 cm × 70 cm (As used in Gusberti et al. [21, 26])			
Current density = 0.75 A/cm^2			
Anode without slots	Measured parameters	Gusberti et al. [21]	Our model
Flat anode	Gas coverage	46.40 %	44.30 %
	Bubble Voltage Drop	299 mV	250 mV
Inclined anode (1.5°)	Gas coverage	41.20 %	38.90 %
	Bubble Voltage Drop	194 mV	205 mV
Current density = 1 A/cm^2, ACD = 40 mm			
Anode without slots	Measured parameters	Gusberti et al. [26]	Our model
Inclined anode (1.5°)	Gas coverage	46.60 %	45.50 %
	Bubble Voltage Drop	330 mV	350 mV
Current density = 1 A/cm^2, ACD = 30 mm (to check the model sensitivity to ACD)			
Anode without slots	Measured parameters	Gusberti et al. [26]	Our model
Inclined anode (1.5°)	Gas coverage	47.80 %	57.70 %
	Bubble Voltage Drop	382 mV	400 mV
	BVD (30 mm) - BVD (40 mm)	**+52 mV**	**+50 mV**

In the next sections, the model will be used for investigating the impact of two anode configurations, based on slot inclination (20 mm and 80 mm), on the gas dynamics around the anode as well as its impact on the bubble voltage drop provoked by the presence of gas phase at its bottom surface throughout the anode lifespan. Anode dimensions used in this study are the same as in our previous work [22] (length: 1690 mm; width: 685 mm). Bath height was 180 mm, including the anode-cathode distance (ACD) of 30 mm. The rounding of different edges of the anode is fixed to 110 mm radius while the rounding of the slot edges is fixed at 50 mm radius.

3.2 Impact of Slot Inclination on Gas Dynamics Throughout Anode Life

For an anode with two longitudinal slots, two configurations have been investigated based on slot inclinations (20 mm and 80 mm) towards the centre channel, Figure 1. It is worth mentioning that throughout its life, anode block shape is related to slot consumption which marks the gas dynamics. For slight inclination of the slot (20 mm), the anode block shape is passing through three stages during its life: the first is when the slot is open (not immersed in the bath); the second is when the slot is fully immersed in the bath; and the third is when the slot is fully consumed (end of anode life). When slots are significantly inclined (80 mm), an additional intermediate stage appears where the slot is partially consumed (intermediate stage between the first and the second stage described above).

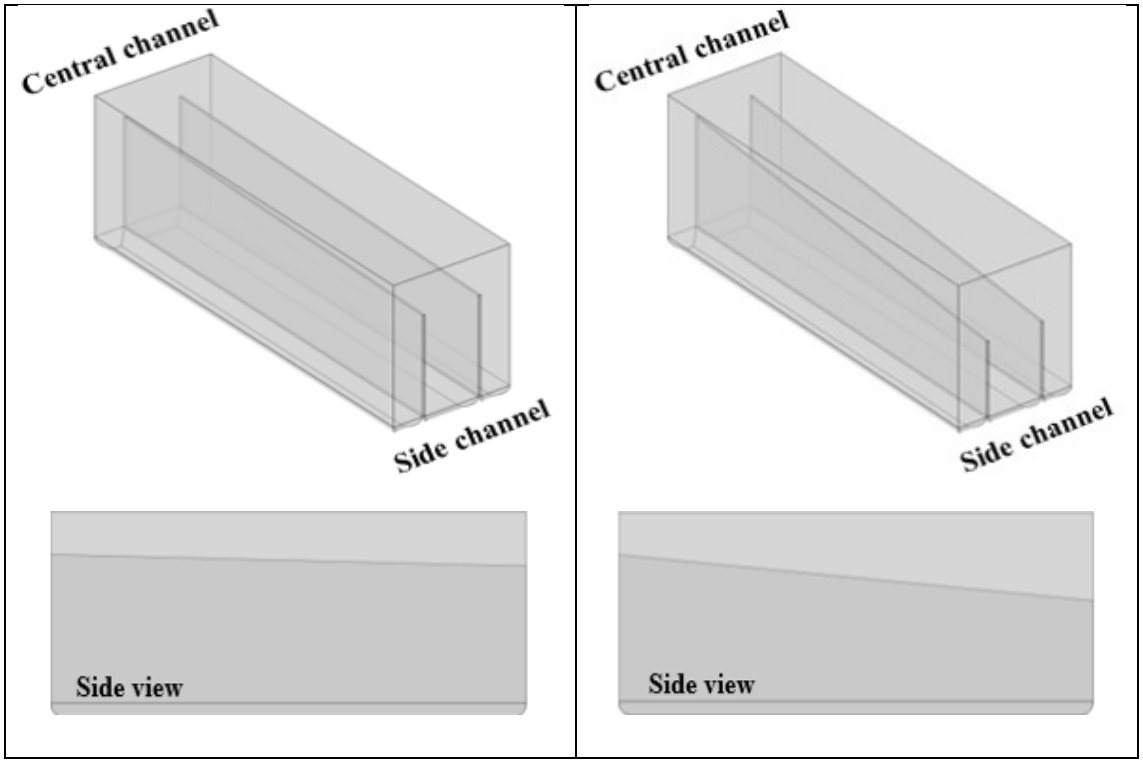

Figure 1. Anode blocks with longitudinal slots. Left: 20 mm inclination, Right: 80 mm inclination.

Figure 2 presents snapshots of the gas concentration distribution in the computational domain for both configurations shown in Figure 1 during the earlier and final stages (corresponding to new anode and end-of-life anode). It is clear that the concentration of the gas underneath the anode is increasing from the early life stage to the end-of-life stage. As explained in our previous paper [22], this is due principally to the fact that during the first stage, the slots are kept open which means that the gas removal from the bottom of the anode is continuous through the open slot and the surrounding channels compared to when the slots are fully consumed (final stage) where the gas has just the surrounding channels to escape through. It is found that this behaviour directly impacts the distribution of the current density as can be seen in Figure 3.

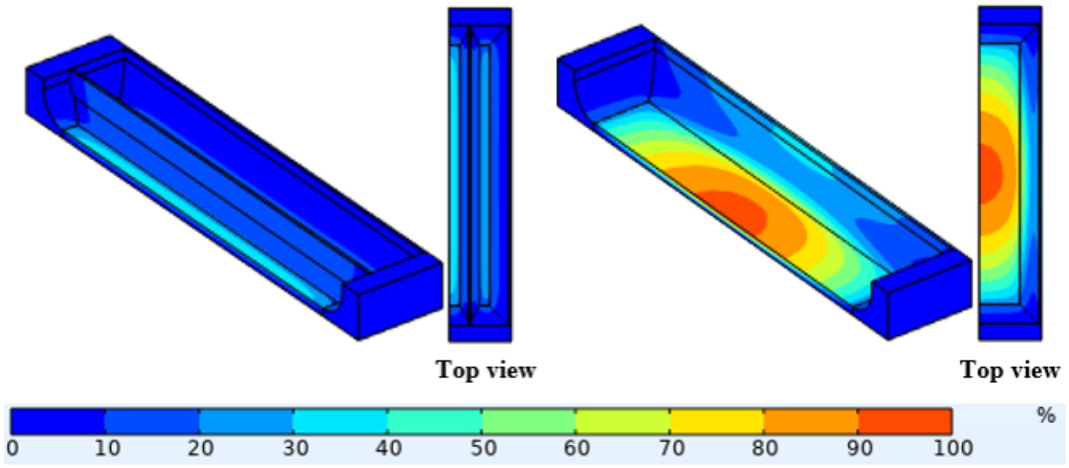

Figure 2. Gas concentration distribution within the computational domain. Left: earlier stage (new anode with open slots), Right: final stage (end-of-life anode with fully consumed slots).

It is remarkable that during the first stage where the slots are still open (Figure 3, left), the current density is almost uniformly distributed at the bottom surface of the anode. This is due to the low gas coverage caused by the continuous removal of the gas from underneath through the open slots as explained before.

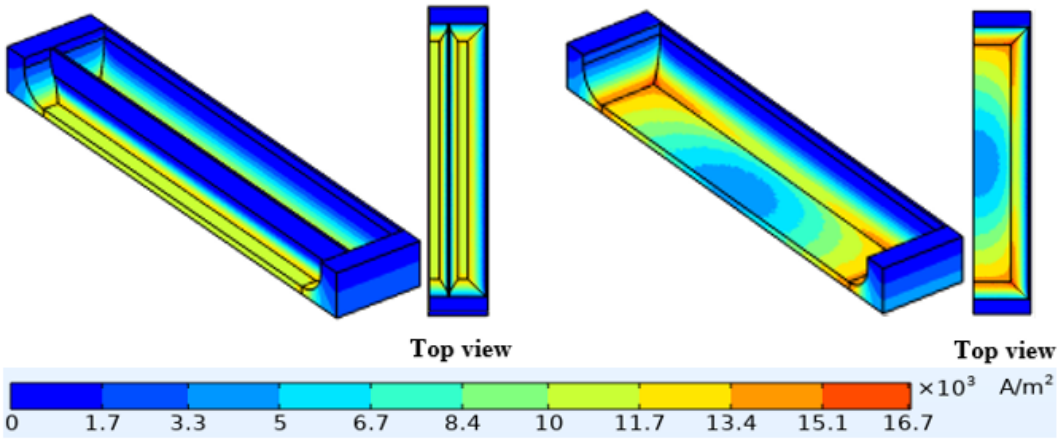

Figure 3. Current density distribution within the computational domain. Left: earlier stage (new anode with open slots), Right: final stage (end-of-life anode with fully consumed slots).

When the slots are fully consumed (end-of-life stage), the gas bubbles coalesce to produce a large volume of gas concentrated at the centre of the anode bottom before reaching the edges of its bottom surface and detaching through the surrounding channels. This explains the redistribution of the current density through the zones away from the centre where the gas coverage is lower, as can be seen in Figure 3 (right). Between these two stages, the slots are fully or partially immersed in the bath (depending on the inclination of the slots).

The next sections detail quantitatively the concentration of the gas underneath the anode and its impact on the bubble voltage drop for the different slot inclinations.

Figure 4 gives the behaviour of the gas concentration at the bottom surface of the anode throughout the anode lifespan for the different slot inclinations (20 mm and 80 mm). It is shown that during the initial phase where the slots are open (lasting ~28 shifts, 9.3 days), the gas concentration below the anode remains constant in different cases (around 28 %).

However, after this period, the concentration under the anode with 80 mm slot inclination begins to rise, while the concentration under the anode with a 20 mm slot inclination stays the same for about 12 more shifts allowing more continuous removal of gas from underneath the anode. The difference is due to the steeper angle of the 80 mm inclined slot. The latter starts to become immersed in the bath earlier than the 20 mm inclined slot. This starts limiting the volume available for gas accumulation provided by the slot, leading to a rise in concentration underneath the anode, as observed in Figure 4.

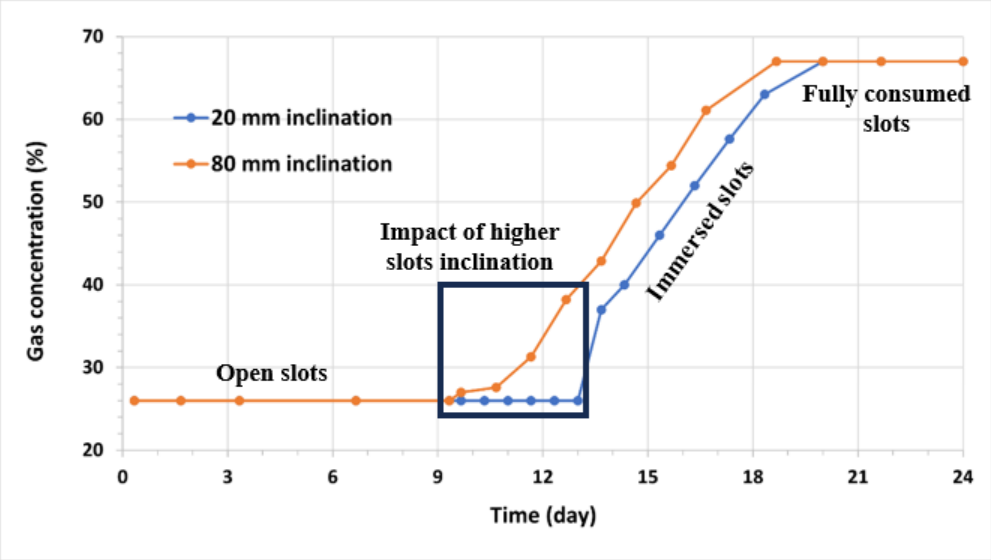

Figure 4. Impact of slot inclination on gas concentration underneath the anode throughout its life.

After about 13 days (39 shifts) (3.7 days after the anode with 80 mm inclined slot, as mentioned above), the slot with a 20 mm inclination starts to be immersed in the bath which explains the rise in the gas concentration at the anode bottom surface from this shift. The gas concentration continues to rise for both cases until the slots are completely consumed (around 20 days, 60 shifts). This marks the beginning of the end-of-life stage, characterized by a high and relatively constant gas concentration for approximately 4 days (12 shifts).

Figure 5 illustrates the variation of the gas voltage drop throughout the anode lifespan. In the first stage, the voltage drop caused by gas coverage remains constant at around 120 mV for roughly 28 shifts (9.3 days) with the 80 mm inclined slot and about 39 shifts (13 days) with the 20 mm inclined slot. As gas coverage increases due to slot immersion, the voltage drop begins to rise. Since the 80 mm slots are immersed before the 20 mm slots, the bubble voltage drop for the 80 mm inclined slot increases before the one with the 20 mm inclined slots.

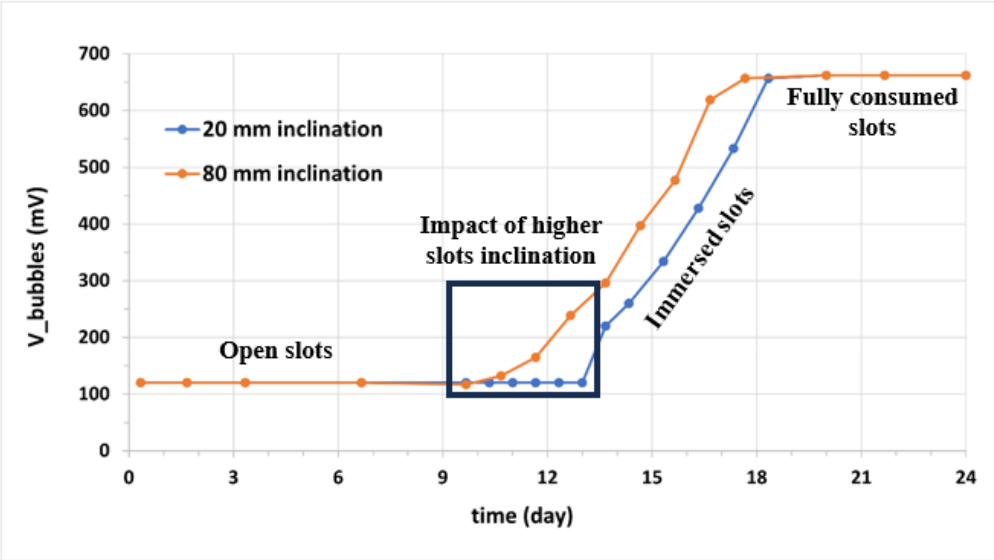

Figure 5. Impact of slot inclination on bubble voltage drop anode throughout its life.

Table 2 summarizes the time-average bubble voltage drop throughout each slot consumption stage for slot inclinations of 20 mm and 80 mm. Throughout the anode lifespan (24 days – 72 shifts), it is found that the average voltage drop in an anode with 80 mm inclined slots is higher by 7 mV than in an anode with 20 mm slot inclination. However, in the immersed slot stage, it is shown that the average bubble voltage drop is lower with highly inclined slots, 80 mm, than with 20 mm inclination. It is worth mentioning that the immersion stage lasts 10.7 days (32 shifts), including ~4 days (12 shifts) of partial immersion, for 80 mm inclination, while it lasts just 7 days (21 shifts) for the 20 mm inclination (with ~0.7 day – 2 shifts of partial immersion). That means that the averages shown in Table 2 for the immersed stage are from day 9.3 to 20 (shift 28 to 60) for 80 mm inclination and from day 13.7 to 20 (shift 41 to 60) for the 20 mm inclination.

Table 2. Time-average bubble voltage drop throughout the anode lifespan for 20 mm and 80 mm slot inclination.

Slot inclination, mm	Slots consumption stage	Number of days (shifts)	Time-average bubble voltage drop, mV	Average voltage drop throughout the anode lifespan
20	New (open slots)	**13 (39 shifts)**	120	**293**
	Immersed (2shifts partially immersed)	**7 (21 shifts)**	405	
	Fully consumed	4 (12 shifts)	662	
80	New (open slots)	**9.3 (28 shifts)**	120	**300**
	Immersed (partially + fully immersed)	**10.7 (32 shifts, (12+20))**	**322**	
	Fully consumed	4 (12 shifts)	662	

Based on the series of numerical simulations in this study, Figure 6 shows a correlation between bubble voltage drop and gas coverage underneath the anode. The observed variations in gas concentration beneath the anode (as discussed previously) are mirrored by changes in gas dynamics throughout the anode lifespan.

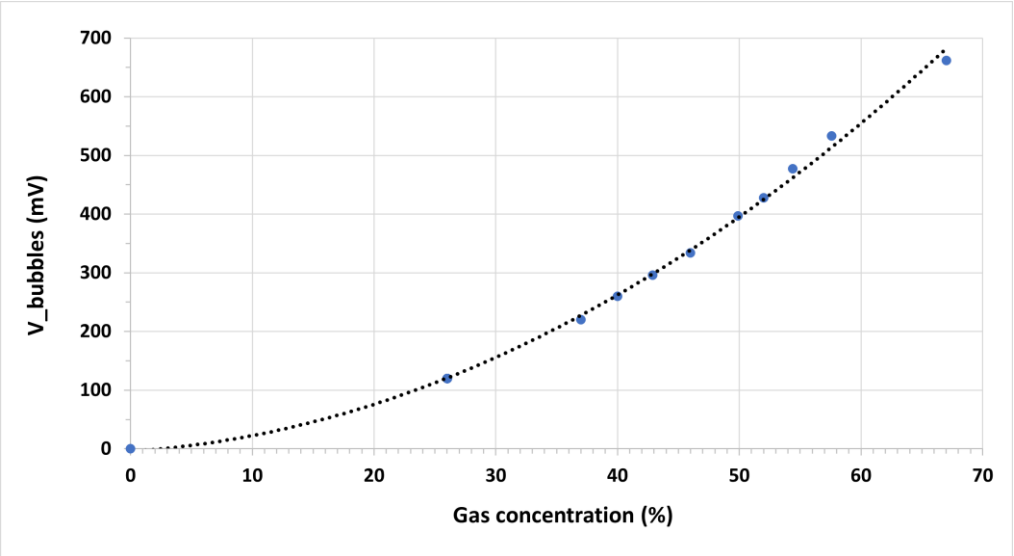

Figure 6. Variation of bubble voltage drop with gas coverage under the anode.

Figure 7 shows the variation of the gas amounts passing through the channels around an anode with 20 mm inclined slots over time. The behaviour is similar to what was depicted earlier for gas concentration under the anode.

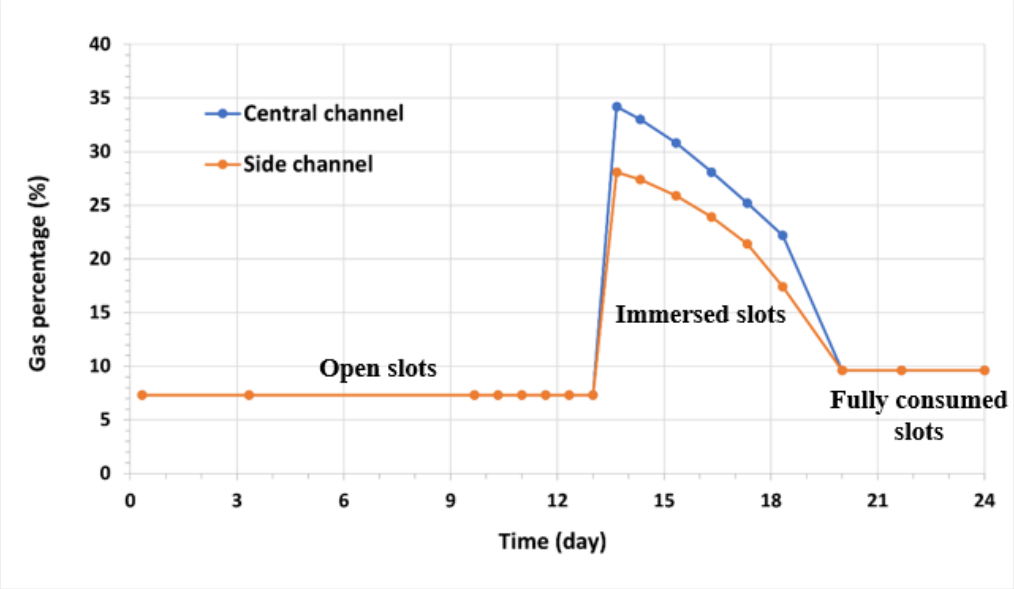

Figure 7. Gas amount through the central and side channels throughout anode life. Anode with 20 mm inclined slots.

The gas flow through the central and side channels can be divided into three stages based on how much of the slots are used up. In the first stage (around 13 days – 39 shifts), the slots are open. This means that most of the gas removed from the bottom surface of the anode passes through the open slots and the inter-anode gap while both central and side channels get about the same small amount of gas (~7 %) directly from the anode bottom. Worthy to be mentioned that in our previous work [22], we found that the gas amount that passes through the central and side channels is ~4 %. This difference is because in our previous model we impose the gas releasing condition just at the bottom surface of the anode which means that the current is all passing through the anode underneath (not distributed through the other surfaces), contrary to the recent model where the current is imposed at all the surfaces in contact with the bath which is more realistic than what was used previously. This allows for some gas generation on the rounded edges, which will escape through the central and side channels.

In the second stage (between days 13 and 20), the slots are immersed into the bath. The top of the slots now blocks the gas from moving out through its top surface (open previously), forcing it to go through the central and side channels instead. At the point where the slots are just completely immersed (day 13.7 – shift 41), the slots can hold the most gas possible (maximum volume provided by the slot to contain removed gases). This is why the total amount of gas going through both channels is highest at this point. Then, the gas amount received by the central and side channels is decreasing throughout the anode life up to day 20 where the slots are fully consumed. It is remarked in this stage that the central channel is always receiving higher amount of gas than the side channel. This is due principally to the effect of the slot inclination towards the central channel. After this (from day 20 onwards), the slots are completely used up, and a constant amount of gas flows through the central and side channels (~9 %).

Significantly increasing the slot inclination (80 mm) alters gas flow behaviour compared to the previous case with a slight inclination (20 mm), as shown in Figure 8. The gas distribution through the central and side channels exhibits four distinct stages, unlike the three stages observed earlier.

The first and the last stage for gas flow remain similar to the 20 mm inclination case. Notably, the first stage in the 80 mm inclination scenario extends for 28 shifts due to earlier immersion triggered by the steeper angle (Table 2).

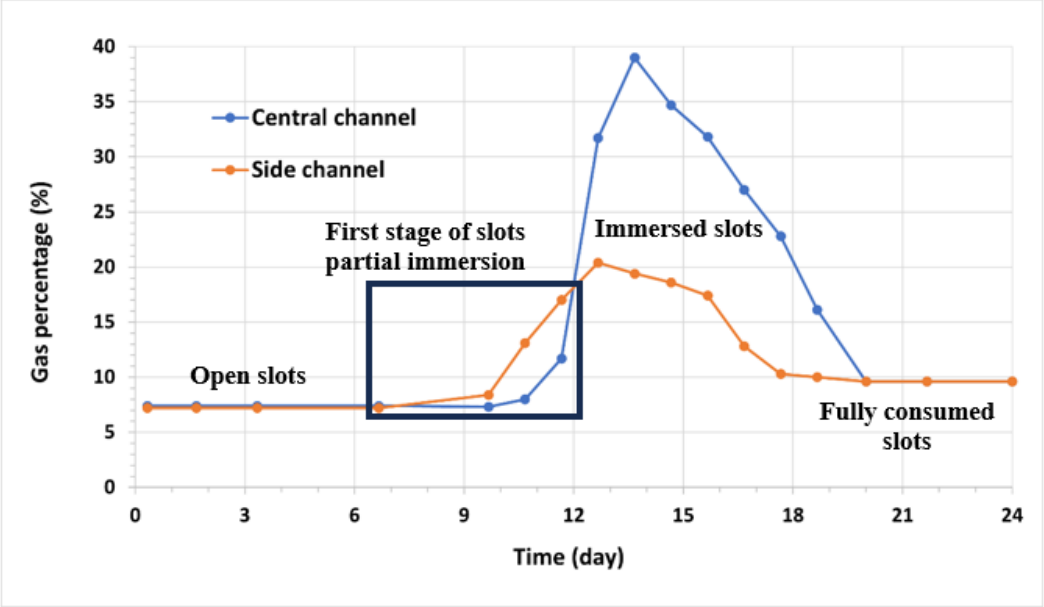

Figure 8. Gas amount through the central and side channels throughout anode life. Anode with 80 mm inclined slots.

When the slot is immersed, two stages are distinct corresponding to the portion size of the immersed slot. Starting at day 9.7 (shift 29), as the slot progressively immersed, gas originally removed from the anode bottom is diverted towards the side channel. Concurrently, until day 10.7 (shift 32), the gas flow through the central channel experiences a marginal decrease compared to the previous stage (when slots are open). This can be explained by the slight decrease in the pressure drop at the central channel when the small part of the slots gets immersed in the side channel region. Afterwards, the gas flow through the central channel begins to recover, but it remains consistently lower than the side channel flow until day 12 – shift 36 (as shown in Figure 8). This limited recovery is primarily because the immersed portion of the slots in the bath (located at the side channel) does not generate enough pressure drop to force a significant amount of gas to pass through the central channel. Figure 9 complements this explanation by illustrating the gas distribution across the slot mid-plane for various days (9.7, 11, and 12). At day 12.3 (shift 37), the partial immersion of the slots would be enough to force a higher quantity of gas to pass through the central channel compared to the side channel, as illustrated in Figure 8.

Starting at day 12.3 (shift 37), the amount of gas directed to the central channel increases, while the amount passing through the side channel decreases. This is because the pressure generated at the steeper side channel becomes higher after day 12.3 (shift 37). This higher pressure creates a larger pressure drop towards the central channel, forcing more gas to flow through it from beneath the anode. This trend continues until day 13.7 (shift 41), when the entire slot is immersed in the bath, maximizing gas flow through the central channel. The gas flow decreases, afterwards, until the slots are completely consumed.

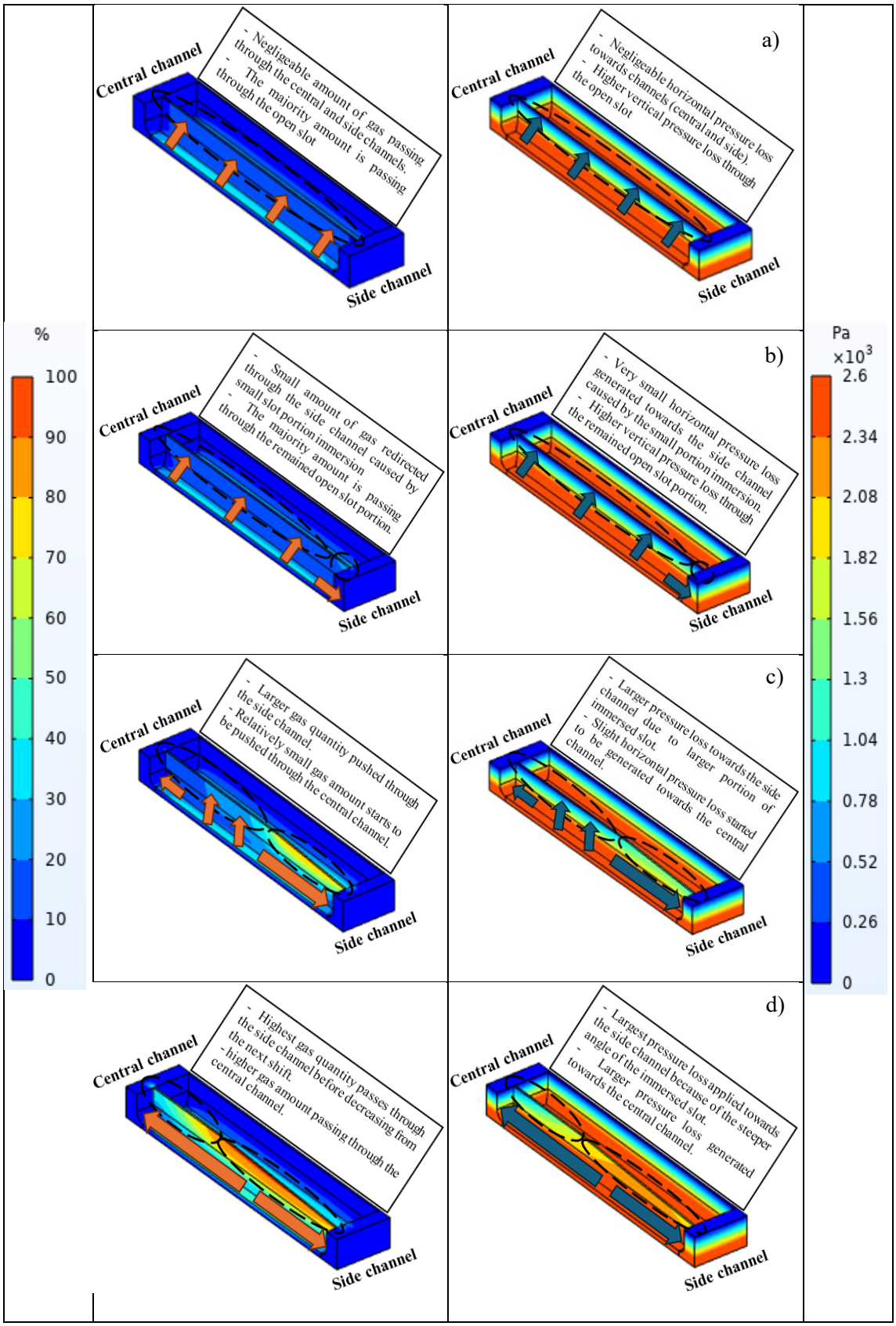

Figure 9. Impact of the slot partial immersion on the gas concentration (left) and the pressure profile (right) within the computational domain; a) open slots; b) day 9.7; c) day 11; d) day 12. Anode with 80 mm inclined slots.

Notably, the slot at the side channel begins to be fully consumed nearly 2.7 days (8 shifts) earlier than those at the central channel area, as shown in Figure 10. This explains why the central channel continues to receive higher amount of gas while the quantity reaching the side channel remains almost constant from day 17.7 (shift 53).

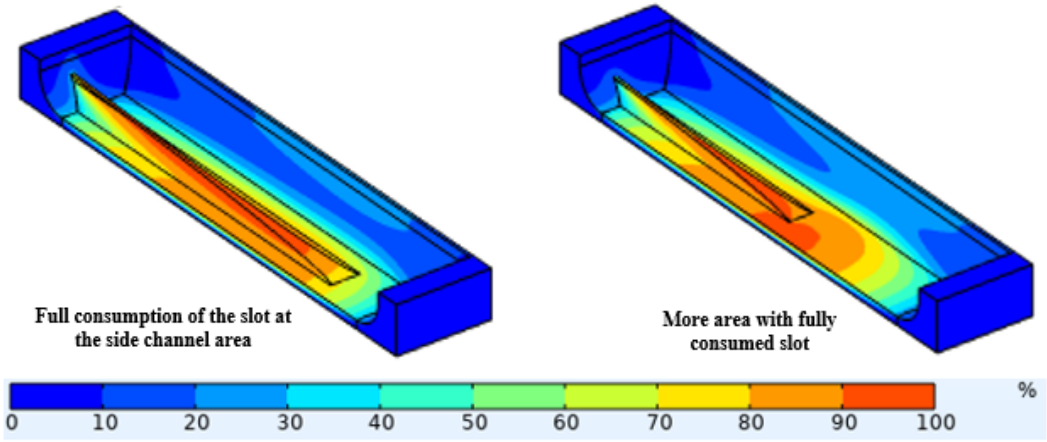

Figure 10. Gas concentration in the computational domain. Left: day 17.7 (shift 53), Right: day 18.7 (shift 56).

Figure 11 shows a comparison between the gas flow at the central channel for both cases (20 mm and 80 mm slot inclination) over the anode life. It shows that the gas dynamics behaviour is almost the same and depends mainly on the slot immersion level.

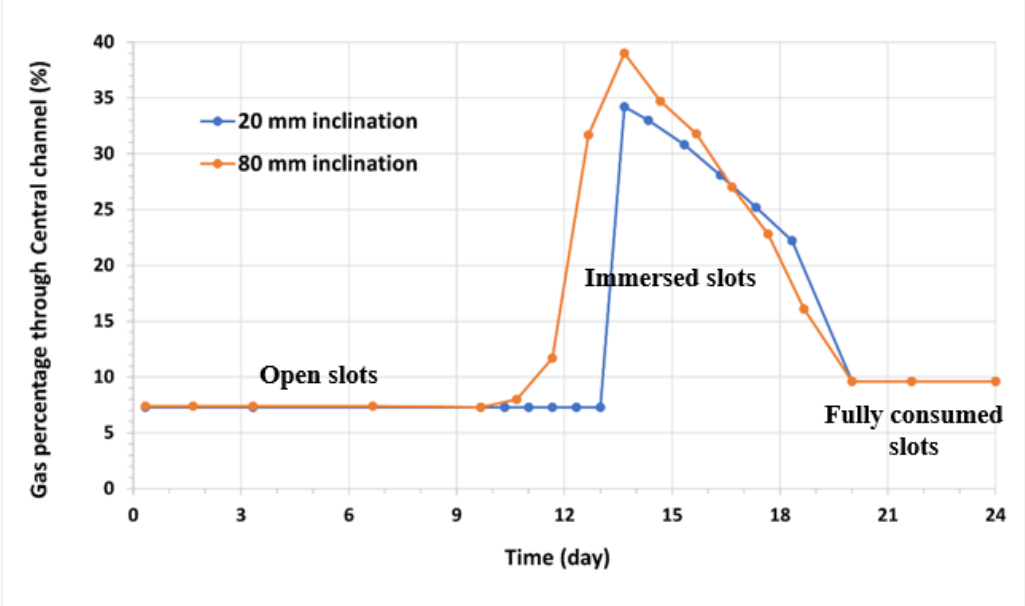

Figure 11. Gas amount through the central channel throughout anode life.

It is depicted that in both cases the gas amount is kept constant at the first stage where the slots are open, rises then till a maximum value while the slots are fully immersed, and reaches finally a constant value after the complete consumption of the slots. The main difference is observed for the number of shifts spent for each stage which was found to be a function of the steepness of the slot angle. It is remarked that for 80 mm inclined slots, the central channel starts receiving a higher quantity of gas ~2 days earlier than the 20 mm inclined slots case. This means, as an example, that the mixing of alumina starts to be helped 2 days earlier with 80 mm inclined slots than with

20 mm inclination. It is also observed that the quantity of the gas received at the central channel is most of the time higher with 80 mm inclination than 20 mm inclination. This is because of the steeper angle of the slots that forces the gas to go principally through the central channel.

The impact of the slot inclination on the gas quantity passing through the side channel throughout the anode lifespan is shown in Figure 12. As explained previously for Figure 11, the gas flow undergoes three different stages depending on the slot immersion. The first and the last stage are obtained when the slots are open or fully consumed, respectively. The intermediate stage is characterized by a variation in the gas quantity passing through.

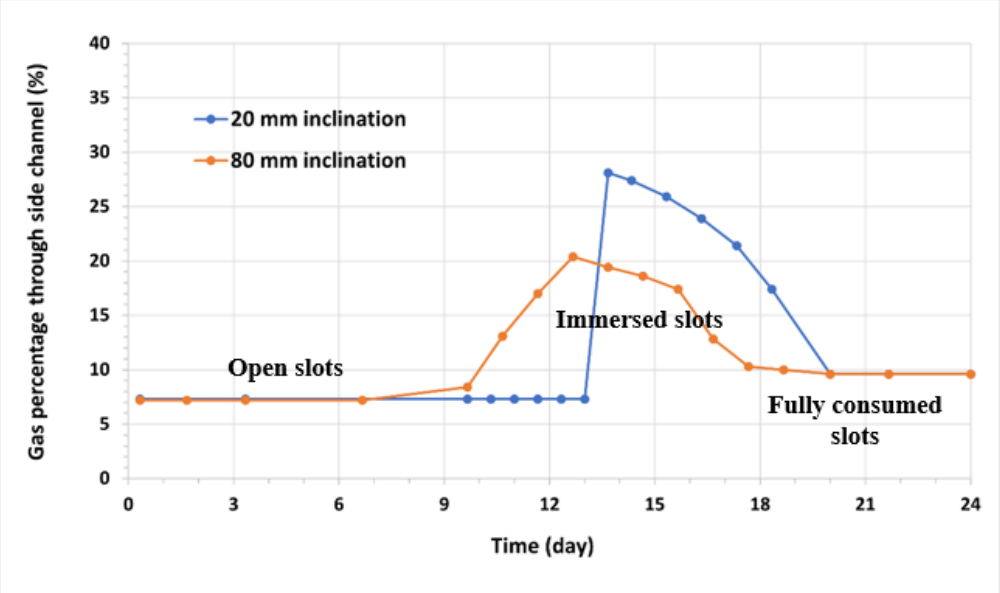

Figure 12. Gas amount through side channel throughout anode life.

When the slot is slightly inclined (20 mm), the first stage lasts for nearly 13 days (39 shifts). The gas amount passing through the side channel increases significantly until day 13.7 (shift 41), at which point the slot becomes fully immersed. Notably, the full immersion process for the slightly inclined slots takes only about 0.7 day (2 shifts). Following full immersion, the gas flow steadily decreases as the slot remains immersed throughout its lifespan until it reaches a constant value, signifying the fully consumed stage. When the 80 mm inclined slot is used, gas redirection to the side channel begins nearly 3.7 days (11 shifts) earlier compared to the 20 mm inclined slots. This is due to the steeper angle of the slot facing the side channel area. The gas flow then increases from day 9.3 to day 12.3 (shift 28 to 37), reaching its maximum at day 12.3 (shift 37). This maximum occurs when the horizontal pressure gradient becomes strong enough to force gas through the central channel (as illustrated in Figure 9d). Interestingly, the 20 mm inclined slot delivers a higher maximum gas amount to the side channel (28 % at day13.7) compared to the 80 mm slot (20 % at day 12.3). Following this peak, the gas quantity decreases until day 17.7 (shift 53), at which point the slot is fully consumed in the side channel area (Figure 10). This full consumption leads to a near-constant value of gas flow through the side channel afterwards.

4. Conclusions

This paper presents a numerical investigation of the impact of the anode slot inclination (20 mm and 80 mm) on the removal and movement of electrolysis gases, primarily carbon dioxide (CO_2), throughout the anode life. It also examines the effect of the inclination on the variation of the bubble voltage drop. Built upon our previous work using COMSOL Multiphysics [22], the upgraded model incorporates the dynamic change in bubble voltage drop over a typical slotted

anode lifespan (~24 days, 72 shifts) by coupling the existing CFD model with the secondary current distribution equation that accounts for both anode reaction kinetics and ohmic losses in the electrolyte. Our results show that the variation of the gas concentration underneath the anode and the generated bubble voltage drop over the anode life follow principally three stages depending on the slot consumption and immersion level. The first stage represents an open slot with low gas concentration and a corresponding lower bubble voltage drop. In contrast, the final stage of fully consumed slots has high gas concentration and the highest bubble voltage drop. The intermediate stage is characterized by an increase in gas concentration **as the slot becomes increasingly immersed, trapping more gas beneath the anode.** This rise in gas concentration leads to a higher bubble voltage drop.

Time-average bubble voltage drop throughout the anode lifespan for higher slot inclination (80 mm) is higher than for 20 mm slot inclination. However, higher slot inclination gives lower average bubble voltage than smaller inclination during the immersion period. This is due to greater number of shifts during which the 80 mm slots remain partially immersed.

Our results also show that the gas distribution through the central and side channels over the anode lifespan depends strongly on the slot inclination and its immersion level. The amount of gas flowing to the central channel is most of the time higher than to the side channel. Higher slot inclination promotes earlier gas flow to the central channel which helps alumina dissolution. Additionally, the peak amount of gas in the side channel is lower with the 80 mm inclination. This suggests that the impact of gas flow on the side ledge is smaller with steeper slots. On the other hand, high slot inclination of 80 mm shows higher time averaged bubble voltage drop (7 mV) than 20 mm inclination; this is a small penalty compared to the benefits of side freeze stability and better alumina dissolution in the central channel.

This model will help optimizing anode slot design in aluminium reduction cells.

5. References

1. Torstein Haarberg, Asbjørn Solheim and Stein Tore Johansen, Effect of anodic gas release on current efficiency in Hall-Heroult cells, *Light Metals* 1998. 475-482.
2. László I. Kiss, Transport processes and bubble driven flow in the Hall-Héroult cell, *Fifth International Conference on CFD in the Process Industries CSIRO,* 13-15 December 2006, Melbourne, Australia.
3. Alton T. Tabereaux and Ray D. Peterson, *Treatise on Process Metallurgy: Industrial Processes*. *Industrial Processes,* Chapter 2.5 - Aluminum Production*,* Volume 3: Industrial processes, 2014, 839-917.
4. Kristian Etienne Einarsrud, Stein Tore Johansen and Ingo Eick, Anodic bubble behaviour in Hall-Héroult cells, *Light Metals,* 2012, 875-880.
5. Bjørn Petter Moxnes, Bjørn Erik Aga and Jørn Hembre Skaar, How to obtain open feeder holes by installing anodes with tracks, *Light Metals,*1998, 247–255.
6. Xinweng Wang et al., Development and deployment of slotted anode technology at Alcoa, *Light Metals,* 2007, 539–544.
7. Stanic Nikolina et al., Bubble phenomena and bubble properties for horizontal and vertical carbon anode surfaces in cryolite melt applying a see-through cell, *Metals*, 2021,965-988.
8. Nolan Richards et al. Characterization of the fluctuation in anode current density and bubble events in industrial reduction cells. *Light Metals,* 2003, 315-322
9. Barry J. Welch, Quantifying PFC emissions from smelter cells, *Proceedings of 10th Australasian Aluminium Smelting Technology Conference*, Launceston, Australia, 9–14 October 2011, Paper 4b3.

10. Stanic Nikolina et al., A Study of Bubble Behavior and Anode Effect on the Graphite and Industrial Carbon Anode in a See-Through Furnace During Aluminium Electrolysis, *Metall Mater Trans B 53*, 2022, 3025–3043, https://doi.org/10.1007/s11663-022-02583-6
11. J. Zoric and A. Solheim, On gas bubbles in industrial aluminum cells with prebaked anodes and their influence on the current distribution, *Journal of Applied Electrochemistry,* 2000, 787-794.
12. Rainier Hreiz et al., Electrogenerated bubbles induced convection in narrow vertical cells: PIV measurements and Euler–Lagrange CFD simulation, *Chemical Engineering Science*, 2015, 138-152.
13. Zhibin Zhao et al., Anodic bubble behaviour and voltage drop in a laboratory transparent aluminum electrolytic cell*, Metall. Mater. Trans. B* 47(3) 2016, 1962–1975.
14. Yipeng Huang et al., Bingliang Gao et al., Anodic bubble behavior in a laboratory scale transparent electrolytic cell for aluminum electrolysis, *Metals,* 2018, 8 (10), 806, https://doi.org/10.3390/met8100806.
15. Liang Wang et al., Numerical modeling of effect of slot on bubble motion in aluminum electrolytic process, *Trans. Nonferrous Met. Soc. China* 28, 2018, 1670−1678.
16. Meijia Sun et al., Effect of slotted anode on gas bubble behaviors in aluminum reduction cell, *Metall Mater Trans B* 48 2017, 3161–3173. https://doi.org/10.1007/s11663-017-1065-y .
17. Meijia Sun, Baokuan Li, Linmin Li, A multi-scale mathematical model of growth and coalescence of bubbles beneath the anode in an aluminum reduction cell, *Metall Mater Trans B* 49, 2018, 2821–2834, https://doi.org/10.1007/s11663-018-1311-y.
18. Meijia Sun, Bao-kuan Li, Zhongqiu Liu, Lixin Tang, Experimental and numerical investigations on transient multiscale bubble behaviors in $CuSO_4$ aqueous solution electrolysis cell, *Chemical Engineering Journal,* 2022, Volume 428, 131182.
19. Poncsák Sándor et al., Study of the Impact of Anode Slots on the Voltage Fluctuations in Aluminium Electrolysis Cells, Using Bubble Layer Simulator, *Light Metals,* 2017, 607-614.
20. Zhu Jiaming et al., CFD Investigation of Bath Flow and Its Related Alumina Transmission in Aluminum Reduction Cells: Slotted Anodes and Busbar Designs, *Metals,* 2020, 10, 805; doi:10.3390/met10060805
21. Vanderlei Gusberti and Dagoberto Schubert Severo, Numerical Modelling of Voltage Drop due to Anode Bubbles, *Proceedings of 41st International ICSOBA Conference*, 5 - 9 November 2023, Dubai, UAE, *Travaux* 52, 1409-1423.
22. Mostafa El Mehdi Brik, Ievgen Necheporenko and Alexander Arkhipov, Impact of Slot Inclination and Thickness on the Distribution of Gas Bubbles Generated below the Anode, *Proceedings of 41st International ICSOBA Conference*, 5 - 9 November 2023, Dubai, UAE, *Travaux* 52, 1425-1438.
23. Alexandre Oury, Modeling Current Distributions in a Molten Salt Electro-Refiner, *COMSOL Blog*, 2015, https://www.comsol.com/blogs/modeling-current-distributions-in-a-molten-salt-electro-refiner, (Accessed on 17 July 2024).
24. Melanie Pfaffe, Which Current Distribution Interface Do I Use, *COMSOL Blog*, 2014, https://www.comsol.com/blogs/current-distribution-interface-use, (accessed on 17 July 2024)
25. Mark Cooksey and William Yang, PIV Measurements on Physical Models of Aluminium Reduction Cells, *Light Metals,* 2006, 359-365.
26. Vanderlei Gusberti and Dagoberto Schubert Severo, Private communication.